Applications of analytical model for characterizing the pear-shaped tribotest for tube hydroforming. Part 2

G Ngaile* and **C Yang**
Department of Mechanical and Aerospace Engineering, North Carolina State University, Raleigh, North Carolina, USA

The manuscript was received on 16 November 2007 and was accepted after revision for publication on 31 March 2008.

DOI: 10.1243/09544054JEM1058

Abstract: Applications of the analytical model for characterizing the pear-shaped tribotest are presented. Details on the derivations of the analytical model can be found in Part 1 of this paper (published in *Proceedings of the Institution of Mechanical Engineers, Journal of Engineering Manufacture*, 2008, Vol. 222). In this test, a tubular specimen is pressurized, forcing the material to flow towards the apex of a pear-shaped die. The height of the pear-shaped tube is a function of the magnitude of friction stress at the tube–die interface. The analytical model is used rapidly to establish the calibration curves for determination of friction coefficient in the pear-shaped tribotest. The model is also used to optimize both process and die geometric variables to suit specific tribological needs. The paper presents examples of how optimal pear-shape tribotest conditions pertaining to die geometry, tubular material properties, tube sizes, and pressure loading can be achieved via this model.

Keywords: tribotest, friction coefficient, tube hydroforming, closed-form equations

1 INTRODUCTION

The main purpose of a tribotest is to provide information on performance characteristics of a lubricant in question. In addition to ranking lubricants and providing friction coefficient values for use in process modelling, the test should accommodate a wide range of variables such as material type, interface pressure level induced, and so on. Depending on the complexity of the tribotest it is sometimes difficult to obtain most of the tribological data by taking experimental measurements. The advances in numerical modelling via finite element analysis (FEA) have opened new avenues where additional tribo data can be acquired. Double cup backward extrusion tribotest is a typical example where by combining the FEA and experiments friction coefficient for the tested lubricant can be determined [**1**–**3**].

The pear-shaped tribotest is commonly used to evaluate lubricant performance for the expansion zone in tube hydroforming. Figure 1 shows the schematic of the test. In this test the fluid is pressurized forcing the material to flow towards the apex of the pear-shaped die. The height of the pear-shaped tube is a measure of the friction stress between the die and the tube [**4**, **5**]. Upon completion of the experiment the protrusion height (PH) is readily measurable and thus lubricants can be ranked instantly. Owing to the complexity of the geometry, however, friction coefficient cannot easily be determined. To obtain friction coefficient, it is necessary to run finite element simulations with different coefficient of friction values and select the simulation that matches with the experiment. As this approach is time consuming it is better to seek an analytical solution.

In Part 1 of this paper an analytical model to characterize the pear-shaped tribotest was presented [**6**]. The analytical model is capable of providing field variables such as pressure distribution at the interface between tube and die, effective stress and strain distribution, and longitudinal and hoop stress/strain distribution. This analytical model provides for a quick way of determining friction coefficient and optimization of the tribo test conditions.

**Corresponding author: Department of Mechanical and Aerospace Engineering, North Carolina State University, Campus Box 7910, Raleigh, NC 27695, USA. email: gracious_ngaile@ncsu.edu; gngaile@eos.ncsu.edu*

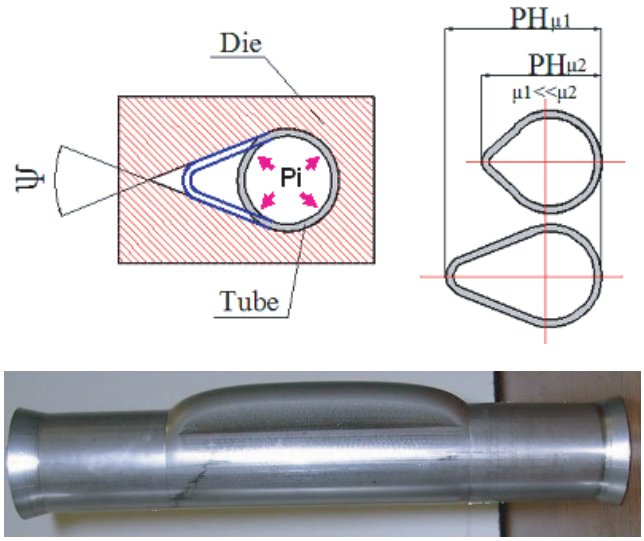

Fig. 1 Pear-shape tribo test

2 OPTIMIZATION OF PEAR-SHAPED TRIBOTEST

In the development of the pear-shaped expansion test, Ngaile *et al.* [**5**] used FEA to determine the best geometry. They simulated various die geometries and came up with a die with vertex angle of 48°. Optimization of a pear-shaped test requires the study of numerous parameters such as die angle, tube size, tube wall thickness, material variables, friction coefficient values, and pressure. Carrying out this parametric study will require extensive simulations. The closed-form solutions established in this study drastically reduce the time and effort in optimizing this test.

The objective function in the optimization of the pear-shaped tribotest is the protrusion height difference ΔPH obtained by imposing two friction conditions, as given in equation (1). The protrusion height difference is influenced by several variables as expressed in equation (2)

$$\Delta\mathrm{PH} = \mathrm{PH}\mu_1 - \mathrm{PH}\mu_2 \tag{1}$$

$$\Delta\mathrm{PH} = f(p, K, n, r, t, \psi) \tag{2}$$

where ΔPH is the change in protrusion height, μ coefficient of friction, p internal pressure, K strength coefficient, n strain hardening exponent, r radius of tube, t tube wall thickness, and ψ pear-shaped die vertex angle. The equations used to establish the friction sensitivity calibration curves (PH versus p) are based on volume constancy, pressure prediction, and geometric relationship between L and PH, see Fig. 2. Details of the derivation are given in Part 1. For brevity some of the equations are recapitulated below.

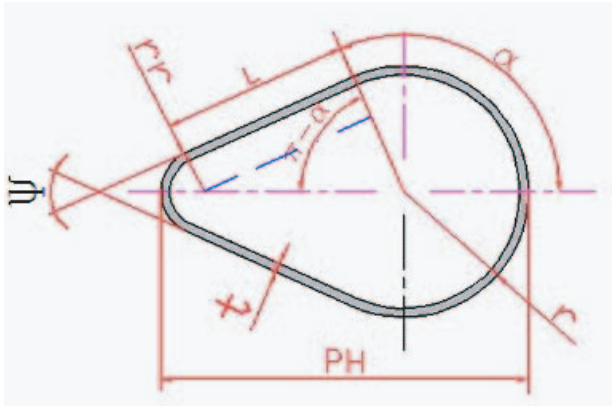

Fig. 2 Geometric parameters for pear-shape expanded tube

1. Volume constant equation

$$\begin{cases} \pi r t_0 = \displaystyle\int_0^{\alpha} rt_0 \\ \quad \times \mathrm{e}^{-\left(\left\{\varepsilon_{\mathrm{N}}^{n} - \left[(\lambda-1)p/K\beta^{n+1}\right]\right\}\mathrm{e}^{\mu(\theta-\alpha)} + \left[(\lambda-1)p/K\beta^{n+1}\right]\right)^{1/n}} \mathrm{d}\theta \\ \quad + \dfrac{(t_0)^2 K\beta^{n+1}}{p\mu}\left\{(\varepsilon_{\mathrm{Q}}{}^{n} - \varepsilon_{\mathrm{N}}{}^{n}) + \displaystyle\sum_{i=1}^{\infty}\frac{(-2)^i}{i!}\frac{n}{n+i}(\varepsilon_{\mathrm{Q}}{}^{n+i} - \varepsilon_{\mathrm{N}}{}^{n+i})\right\} \\ \quad + (r - L\mathrm{ctg}(\pi-\alpha))(\pi-\alpha)t_0\mathrm{e}^{-\varepsilon_{\mathrm{Q}}} \\ \quad \frac{1}{n}(\varepsilon_{\mathrm{Q}}{}^{n} - \varepsilon_{\mathrm{N}}{}^{n}) + \displaystyle\sum_{i=1}^{\infty}\frac{(-1)^i}{i!}\frac{1}{i+n}(\varepsilon_{\mathrm{Q}}{}^{i+n} - \varepsilon_{\mathrm{N}}{}^{i+n}) = \frac{\mu p}{K\beta^{n+1} n t_0} L \end{cases} \tag{3}$$

2. Pressure prediction

$$p = \frac{K\beta^{n+1}\varepsilon_{\mathrm{Q}}{}^{n} t_0 \mathrm{e}^{-\varepsilon_{\mathrm{Q}}}}{r - L\mathrm{ctg}(\pi-\alpha)} \tag{4}$$

3. Geometrical relationship between L and PH

By trigonometric manipulation, equations (5) and (6) can be obtained

$$rr = r - L\mathrm{ctg}(\pi-\alpha) \tag{5}$$

$$L = \frac{\mathrm{PH} - 2r}{\mathrm{csc}(\pi-\alpha) - ctg(\pi-\alpha)} \tag{6}$$

Combining equations (3), (4), (5), and (6) equation group (7) can be obtained

$$\begin{cases} \pi r t_0 = \displaystyle\int_0^{\alpha} rt_0 \mathrm{e}^{-\left(\left\{\varepsilon_{\mathrm{N}}{}^{n} - \left[(\lambda-1)p/K\beta^{n+1}\right]\right\}\mathrm{e}^{\mu(\theta-\alpha)} + \left[(\lambda-1)p/K\beta^{n+1}\right]\right)^{1/n}} \mathrm{d}\theta \\ \quad + \dfrac{(t_0)^2 K\beta^{n+1}}{p\mu}\left\{(\varepsilon_{\mathrm{Q}}{}^{n} - \varepsilon_{\mathrm{N}}{}^{n}) + \displaystyle\sum_{i=1}^{\infty}\frac{(-2)^i}{i!}\frac{n}{n+i}(\varepsilon_{\mathrm{Q}}{}^{n+i} - \varepsilon_{\mathrm{N}}{}^{n+i})\right\} \\ \quad + (r - L\mathrm{ctg}(\pi-\alpha))(\pi-\alpha)t_0\mathrm{e}^{-\varepsilon_{\mathrm{Q}}} \\ \dfrac{p}{K\beta^{n+1}}\dfrac{\mu}{n t_0} L = \dfrac{1}{n}(\varepsilon_{\mathrm{Q}}{}^{n} - \varepsilon_{\mathrm{N}}{}^{n}) + \displaystyle\sum_{i=1}^{\infty}\frac{(-1)^i}{i!}\frac{1}{i+n}(\varepsilon_{\mathrm{Q}}{}^{i+n} - \varepsilon_{\mathrm{N}}{}^{i+n}) \\ p = \dfrac{K\beta^{n+1}\varepsilon_{\mathrm{Q}}{}^{n} t_0 \mathrm{e}^{-\varepsilon_{\mathrm{Q}}}}{r - L\mathrm{ctg}(\pi-\alpha)} \\ L = \dfrac{\mathrm{PH} - 2r}{\mathrm{csc}(\pi-\alpha) - ctg(\pi-\alpha)} \end{cases} \tag{7}$$

From equation (7) when the geometric dimensions r, t, α, and λ, material properties, K and n, and process

parameters p, and μ are known, then there are four unknown variables: PH, ε_N, ε_Q, and L which can be solved mathematically. By solving equation (7) friction sensitivity profile can be obtained. Figure 3(a) shows an example of a friction sensitivity profile for a pear die shape with a vertex angle $\psi = 48°$ and 34.93 mm diameter tubular specimen. This curve shows protrusion height difference between two friction conditions; $\mu_1 = 0.05$ and $\mu_2 = 0.10$. FEA results from DEFORM 2D software are also plotted. Figure 3(a) shows that the protrusion height difference initially increases with increase in pressure, but then starts to decrease. This variation in protrusion height difference ΔPH with change in p implies that there is an optimal pressure associated with higher frictional sensitivity of the tribotest.

The occurrence of optimal pressure which corresponds to maximum protrusion height change is caused by the material flow characteristic towards the apex. Figure 3(b) shows velocity profiles of material flow along the die–tube contact region and non-contact region for different pressure levels. These profiles were obtained from FEA for $\mu = 0.05$. It can be observed from Fig. 3(b) that at pressure levels of 60 MPa and 80 MPa hoop velocity between the two regions exhibit linear increase from the bottom of a pear-shaped tube to the apex (P1 to P54). However, when the pressure level exceeds 90 MPa the hoop velocity from P1 to P54 is non-linear. That is, the rate of increase of the hoop velocity in the contact region decreases with an increase in pressure. At 130 MPa and 140 MPa, the material movement for a large portion of the die–tube contact region approaches zero. As a result, friction sensitivity decreases. Thus Fig. 3(a) shows that beyond 90 MPa the increment of protrusion height is largely dominated by rapid thinning in the free expansion region.

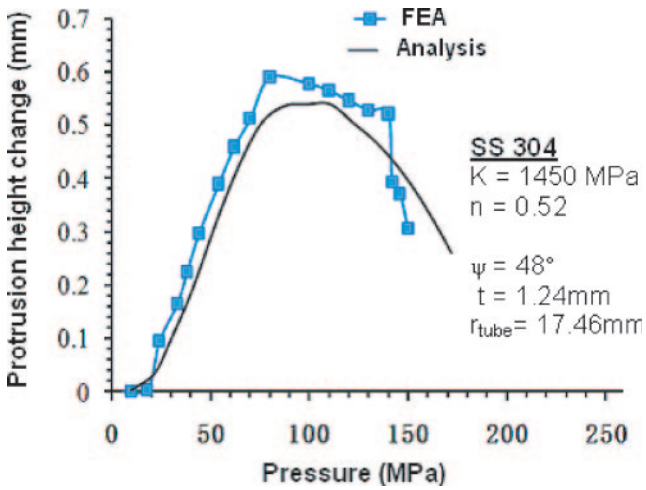

Fig. 3(a) Friction sensitivity profile

To gain better insight of the characteristics of the pear-shaped expansion tribotest, a parametric study was conducted. Table 1 shows the variables that were used in the model to study:

(a) the influence of vertex angle ψ on ΔPH;
(b) the influence of strain hardening exponent on ΔPH;
(c) the influence of tube wall thickness on ΔPH;
(d) the influence of tube radius on ΔPH.

2.1 Influence of vertex angle ψ on ΔPH

Parametric study was carried out under the following conditions:

(a) varying Pi from 10 MPa to 110 MPa;
(b) varying ψ from 30° to 60° at intervals of 6°;
(c) friction coefficients $\mu_1 = 0.05$ and $\mu_2 = 0.10$;
(d) $K = 1450$ MPa and $n = 0.52$;
(e) $r = 28.5$ mm and $t = 1.6$ mm.

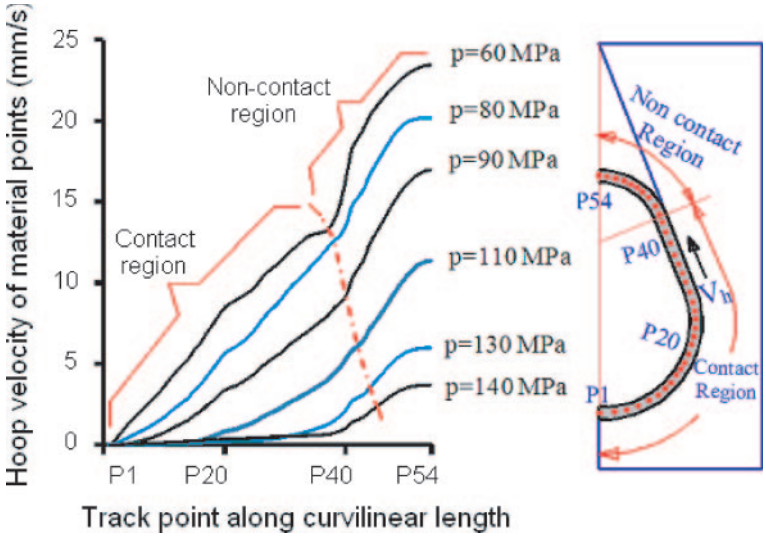

Fig. 3(b) Velocity profiles of material points along the die for various pressure levels

Table 1 Variables used in the parametric study

Geometric variables	ψ	30°, 36°, 42°, 48°, 54°, 60°
	r	14.25 mm, 28.5 mm, 57 mm
	t	0.8 mm, 1.6 mm, 3.2 mm
Process variables	P	10 MPa–110 MPa
	μ	0.05, 0.1
Material variables	K	1450 MPa
	n	0.1, 0.2, 0.3, 0.4, 0.5, 0.6

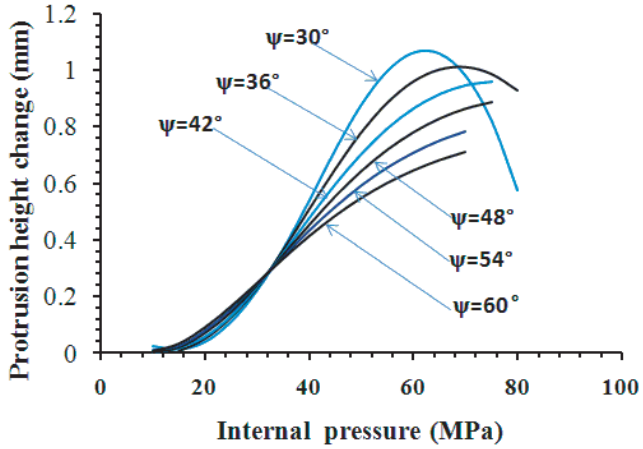

Fig. 4 Influence of vertex angle on protrusion height difference between $\mu_1 = 0.05$ and $\mu_2 = 0.10$

Figure 4 depicts a family of curves for protrusion height difference between $\mu_1 = 0.05$ and $\mu_2 = 0.10$ for different vertex angles. Figure 4 shows that the protrusion height difference initially increases with increase in pressure, but then starts to decrease. This variation in protrusion height difference ΔPH with change in Pi implies that there is an optimal pressure associated with higher frictional sensitivity of the tribotest. Figure 4 indicates that maximum ΔPH/*friction sensitivity* decreases with the increase of vertex angle. However, Fig. 4 also shows that with decrease in the vertex angle, the curve (ΔPH versus *p*) becomes steeper, which means that the selectable test pressure band Pb becomes smaller. The pressure band concept is illustrated in Fig. 5. Care should therefore be taken in selecting an optimal die vertex angle, which corresponds to the effective pressure band for the tribotests. As shown in Fig. 5, for a desired test pressure band Pb, a friction sensitivity profile which is determined by the die vertex angle ψ, should be chosen such that the intersections at P_1 and P_2 are not far away from the ΔPH associated with P_{opt}.

2.2 Influence of strain hardening exponent *n* on ΔPH

There are various tubular materials used in THF. These materials have different strain hardening values. Thus, it is important to determine how

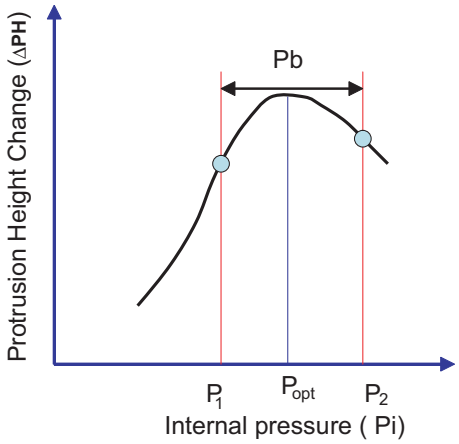

Fig. 5 Effective test pressure band as related to friction sensitivity profile

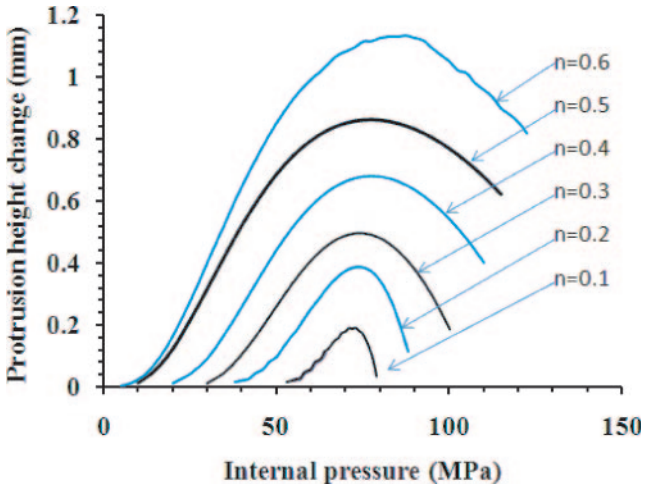

Fig. 6 Influence of strain hardening on protrusion height difference between $\mu_1 = 0.05$ and $\mu_2 = 0.10$ for $\psi = 48°$

strain hardening influences friction sensitivity of the pear-shaped test. Parametric study was carried out under conditions:

(a) varying Pi from 10 MPa to 110 MPa;
(b) friction coefficients $\mu_1 = 0.05$ and $\mu_2 = 0.10$;
(c) $K = 1450$ MPa, $n = 0.1$, 0.2, 0.3, 0.4, 0.5, and 0.6;
(d) $r = 28.5$ mm, $t = 1.6$ mm, and $\psi = 48°$;
(e) maximum wall thinning was set at 30 per cent.

Figure 6 shows that the protrusion height difference increases with an increase in strain hardening exponent. This implies that more care should be taken when evaluating lubricants using tubular materials with lower strain hardening exponent.

2.3 Influence of tube wall thickness on ΔPH

Parametric study was carried out under conditions similar to those used for studying the influence of

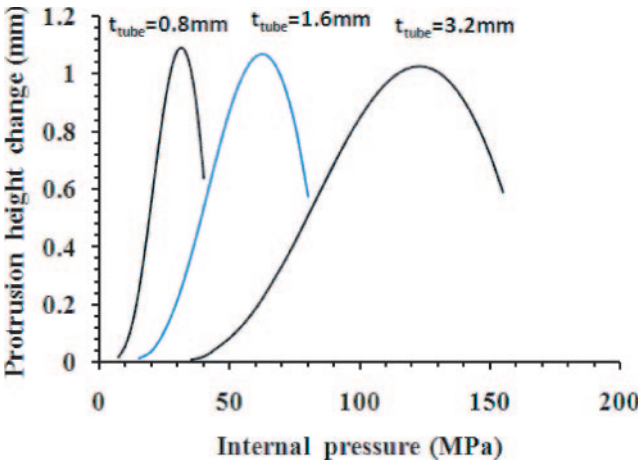

Fig. 7 Influence of tube wall thickness on protrusion height difference

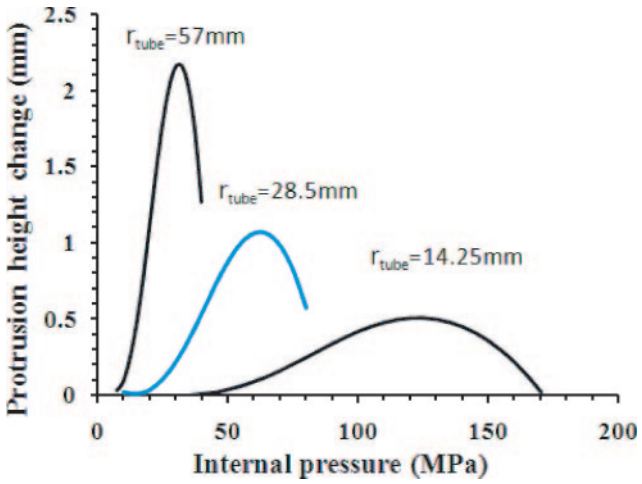

Fig. 8 Influence of tube radius on protrusion height difference, $\psi = 30^\circ$

strain hardening. Additional parameters for this study were:

(a) $t = 0.8$ mm, 1.6 mm, and 3.2 mm;
(b) $r = 28.5$ mm;
(c) $K = 1450$ and $n = 0.52$;
(d) $\psi = 30^\circ$.

Figure 7 shows a family of curves for ΔPH for the different wall thicknesses $t = 0.8$ mm, 1.6 mm, and 3.2 mm. The three profiles in Fig. 7 are for die vertex angle of 30°. Other die vertex angles resulted in similar patterns. Figure 7 shows that the influence of thickness on protrusion height difference is insignificant. The protrusion height differences for $t = 0.8$ mm, $t = 1.6$ mm, and $t = 3.2$ mm using a die with vertex angle of 30° are 1.06 mm, 1.02 mm, and 1.01 mm, respectively.

2.4 Influence of tube radius on ΔPH

Parametric study was carried out under conditions similar to those used for studying the influence of wall thickness. Additional parameters for this study were $r = 14.25$ mm, 28.5 mm, 57 mm, $t = 1.6$ mm, $K = 1450$, $n = 0.52$, and $\psi = 30^\circ$. Figure 8 shows a drastic increase of protrusion height difference with an increase in tube radius. The figure shows that a die vertex angle of 30° resulted in protrusion height differences of 2.14 mm, 1.06 mm, and 0.52 mm for tube radii 57 mm, 28.5 mm, and 14.25 mm, respectively. In other words, the friction sensitivity increases by about 100 per cent when tube radius doubles as to be expected from geometrical scaling consideration. The protrusion height difference is associated with the change in friction coefficient from $\mu_1 = 0.05$ to $\mu_2 = 0.10$.

2.5 Interface pressure loading

In a tribotest, the performance of the lubricant is also measured upon the maximum pressure it can withstand before failure. Furthermore, the interface pressure distribution at the tool can be used to study wearing characteristic of the die. Under the pear-shaped test two distinct pressure distributions are observed at the tube–die interface: region AB, which is the arc section of the die exhibits lower interface pressure, as compared to the region BC (linear section of the die). Figure 9 shows that for the internal fluid pressure Pi = 36 MPa the average pressure in the arc region was 6 MPa which is about 83 per cent lower than 36 MPa exhibited at the linear die section. At Pi = 62 MPa, the arc section experienced interface pressure of 23 MPa, which is 64 per cent lower than 62 MPa exhibited at the linear section.

3 PREDICTION OF FRICTION COEFFICIENT

Equation group (7) can be rearranged to obtain equation (8) where internal pressure p is normalized with K

$$\begin{cases} \pi r t_0 = \int_0^\alpha r t_0 \mathrm{e}^{-\left(\left\{{\varepsilon_\mathrm{N}}^n - \frac{(\lambda-1)p}{K\beta^{n+1}}\right\}\mathrm{e}^{\mu(\theta-\alpha)} + \left[\frac{(\lambda-1)p}{K\beta^{n+1}}\right]\right)^{1/n}} \mathrm{d}\theta \\ \qquad + \frac{(t_0)^2\beta^{n+1}}{(p/k)\mu}\left\{({\varepsilon_\mathrm{Q}}^n - {\varepsilon_\mathrm{N}}^n) + \sum_{i=1}^{\infty}\frac{(-2)^i}{i!}\frac{n}{n+i}({\varepsilon_\mathrm{Q}}^{n+i} - {\varepsilon_\mathrm{N}}^{n+i})\right\} \\ \qquad + (r - L\mathrm{ctg}(\pi-\alpha))(\pi-\alpha)t_0\mathrm{e}^{-\varepsilon_\mathrm{Q}} \\ \frac{p}{K}\frac{\mu}{\beta^{n+1}nt_0}L = \frac{1}{n}({\varepsilon_\mathrm{Q}}^n - {\varepsilon_\mathrm{N}}^n) + \sum_{i=1}^{\infty}\frac{(-1)^i}{i!}\frac{1}{i+n}({\varepsilon_\mathrm{Q}}^{i+n} - {\varepsilon_\mathrm{N}}^{i+n}) \\ p/K = \frac{\beta^{n+1}{\varepsilon_\mathrm{Q}}^n t_0 \mathrm{e}^{-\varepsilon_\mathrm{Q}}}{r - L\mathrm{ctg}(\pi-\alpha)} \\ L = \frac{\mathrm{PH} - 2r}{\mathrm{csc}(\pi-\alpha) - \mathrm{ctg}(\pi-\alpha)} \end{cases} \quad (8)$$

In equation group (8), if dimensions r, t, and α and material properties K and n are known, there remain only six unknown variables: PH, L, p, μ, ε_N, and ε_Q. Because the internal pressure PI and protrusion height PH can be obtained from experiment, the unknown variables in equation (8) are L, μ, ε_N, and ε_Q. Thus, equation group (8) can be solved to obtain μ.

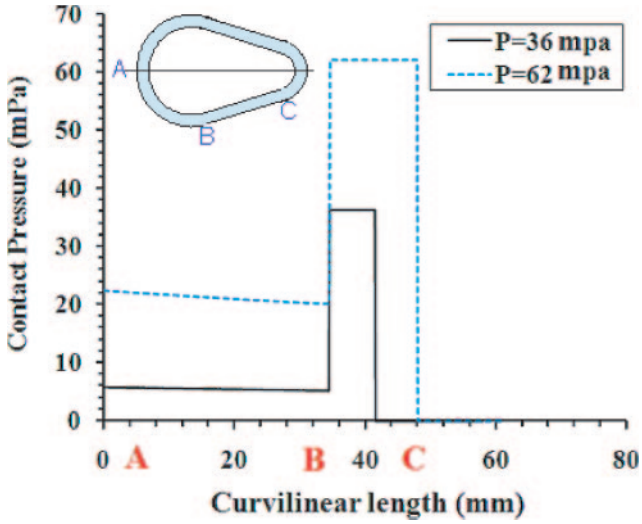

Fig. 9 Tube–die interface pressure variations

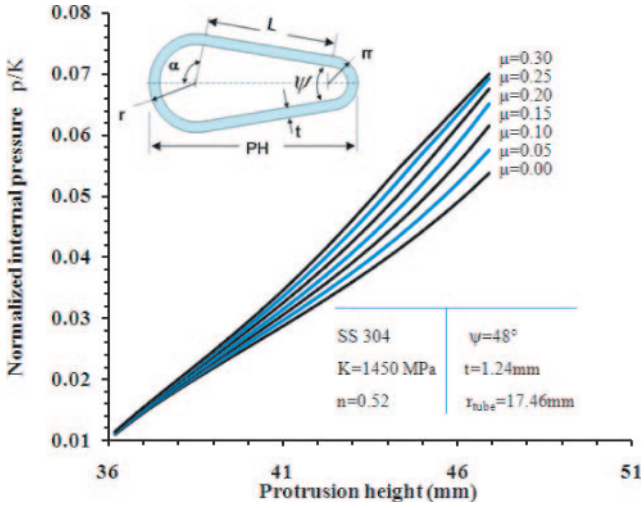

Fig. 10 Friction calibration chart

However, μ cannot be determined explicitly; a calibration chart is therefore used to estimate μ. The calibration chart is composed of a family of curves (PH versus p/K) for different friction coefficient values. Figure 10 shows an example of a friction calibration chart for a pear-shaped expansion test for tube material $n = 0.52$, $r = 17.46$ mm, $t = 1.24$ mm, and die vertex angle $\psi = 48°$. By superimposing on a graph the ratio p/K and protrusion height PH obtained from pear-shaped tribotest experiments, the friction coefficient for a tested lubricant can be determined. Note that the friction calibration chart is dependent on material properties n, die geometry, and tube size and independent of K.

4 PEAR-SHAPE EXPANSION TESTS

Pear-shaped expansion tests were carried out with different lubrication conditions and the calibration charts were used to estimate friction coefficients. The experimental results were also used to validate the analytical model.

Fig. 11 Hydroforming test rig

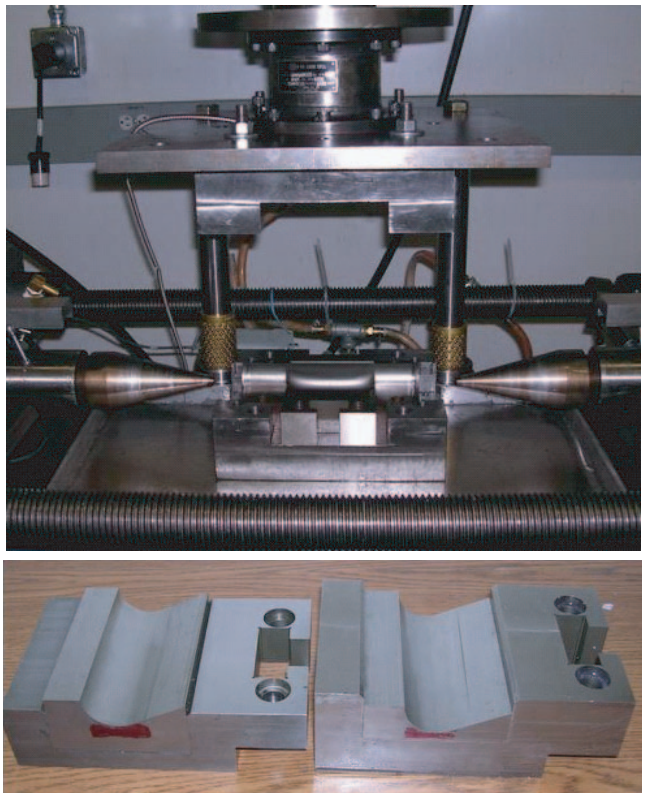

Fig. 12 Hydroforming tooling

4.1 Test set-up and experimental procedures

The experimental set-up for the pear-shaped tribotest is shown in Figs 11 and 12. The test set-up consists of the upper die, lower die, and two axial

Table 2 Test matrix

Tube material	Lubricants	Number of specimens
SS 304 $\Phi = 34.93$ mm	Teflon sheet	2
$t = 1.24$ mm	Polymer	2
	No-lub	2
$\Phi = 57.15$ mm	Teflon sheet	2
t = 2 mm	Polymer	2
	No-lub	2

cylinders. The upper die is connected to 150 ton hydraulic press through a 150 ton load cell. The lower die seats on a table. The dies are made of A2 steel and hardened to 62 HRC. Table 2 shows the test matrix. Two sizes of stainless steel tubing (SS 304) and two lubricants were used in the tribotests. The small tubing had an outer diameter of $\Phi = 34.93$ mm and wall thickness of $t = 1.24$ mm, while the larger tubing had outer diameter of $\Phi = 57.15$ mm and wall thickness of $t = 2$ mm. In order to use the same fluid pressure loading, the tube sizes were selected such that the radius to thickness ratio, λ, is approximately equal to 14.

Two lubricants, teflon sheet, and polymer-based lubricants were used in the test (Table 2). The polymeric lubricant used is based on steryl methacrylate/methyl methacrylate. Details on the composition of the polymeric lubricant can be found in reference [**7**]. The specimens were cut to 205 mm long and were cleaned with acetone before applying the lubricant. The polymeric lubricant was applied by a brush while with Teflon lubricant, Teflon sheet of 0.12 mm thick was wrapped around the specimen. During the test fluid pressure was ramped linearly from 0 MPa to 67 MPa in 30 s.

4.2 Test results and discussion

Figure 13 shows sets of specimens for smaller and larger tubing after testing. The protrusion heights were measured for all samples and the average protrusion heights were plotted in Fig. 14 for small and large tubing. Figure 14 shows that Teflon lubricant resulted in large protrusion height of 44.6 mm followed by polymeric lubricant with a protrusion height of 44 mm. The specimens formed without lubricant exhibited an average height of 43 mm. Similarly, with larger tubing Teflon lubricant exhibited the largest protrusion height of 70.7 mm followed by polymeric lubricant with a protrusion height of 69.6 mm. The non-lubricated specimens resulted in a protrusion height of 68.7 mm. It should be noted that plane strain condition was not fully established with large tubing ($\Phi = 57.15$ mm) used in the experiment because the bulge width was too short. This was attributable to the limitations of the current tooling. However, as

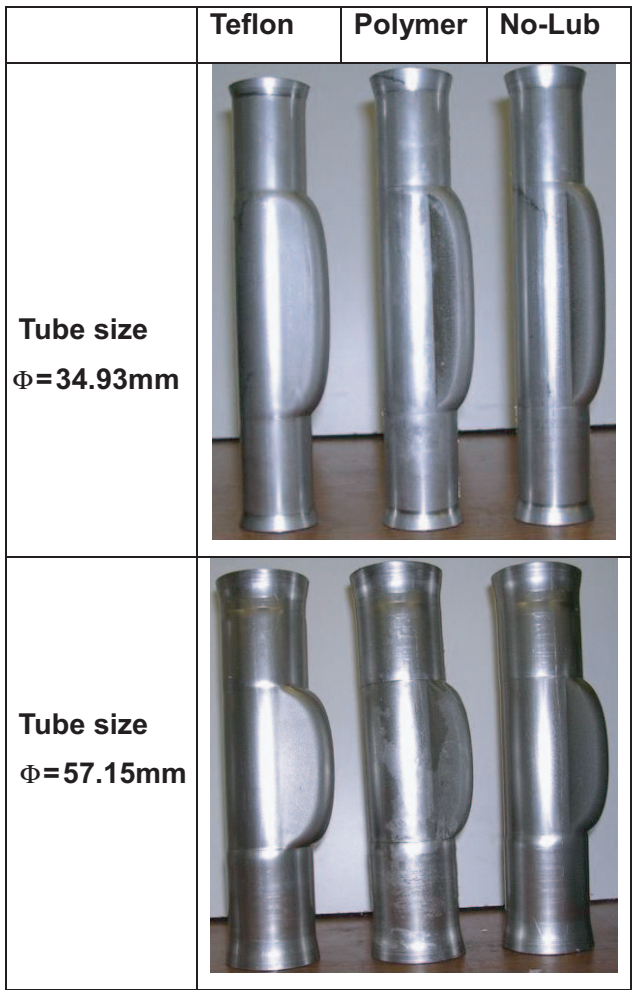

Fig. 13 Pear-shaped hydroformed tubes

seen in Fig. 13 fully plane strain condition was achieved for small tubing.

The difference in the protrusion height between specimens hydroformed with Teflon and No-lub conditions for smaller tubing is 1.6 mm. The large tubing resulted in a protrusion height difference of 2 mm. The larger protrusion height is as discussed earlier owing to geometric scaling. It agrees with the results from the analytical model discussed in section 2.4 where it was shown that friction sensitivity increases with increase in tube size.

Calibration curves were used to determine the friction coefficient of the tested lubricant friction. Figure 15 shows friction calibration curves with superimposed protrusion height values obtained from experiment for the three lubrication conditions. From the calibration curves the friction coefficients for Teflon and polymeric lubricants were estimated to be $\mu = 0.08$ and $\mu = 0.14$ respectively. The calibration curves show that friction coefficients of under $\mu = 0.30$ were exhibited when no lubricant was used.

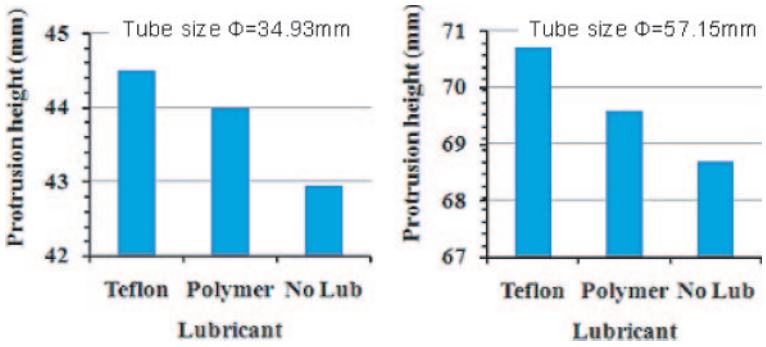

Fig. 14 Influence of lubricants on protrusion height for tube size $\Phi = 34.93$ mm, and $\Phi = 57.15$ mm

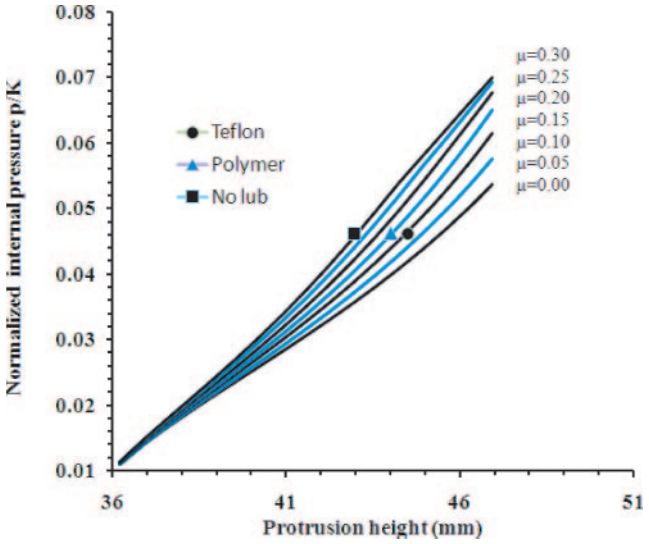

Fig. 15 Estimated friction coefficient for Teflon and polymer lubricants

5 CONCLUSIONS

Potential applications of the analytical model for characterizing the pear-shaped tribotest were presented. Besides facilitating the determination of friction coefficient for tested lubricants, the analytical model has proved to be a useful tool in rapid optimization of pear-shaped tribotest conditions.

The analytical model also provides a clear picture of the local pressure loading distribution on the tube–die interface. This tribo-information can be used in studying wear characteristics of hydroforming dies as a function of lubricant type, pressure levels, and pressure gradients at the tube–die interfaces.

Hydroforming experiments carried out with two lubricants have demonstrated how friction coefficient values for tested lubricants can be estimated using the established calibration curves. The experiments also demonstrated that the friction sensitivity of the pear-shaped tribotest increases with increase in the diameter of tubular specimens. This is an important consideration, particularly when evaluating lubricants using tubular materials with a lower strain hardening exponent.

ACKNOWLEDGEMENT

The authors would like to acknowledge the National Science Foundation, through which this work was funded under Project No. DMI-0448885.

REFERENCES

1 **Buschhausen, A., Weinmann, K., Lee, J. Y.,** and **Altan, T.** Evaluation of lubrication and friction in cold forging using a double backward-extrusion process. *J. Mater. Process. Technol.*, 1992, **33**, 95–108.

2 **Schrader, T., Shirgaokar, M.,** and **Altan, T.** A critical evaluation of the double cup extrusion test for selection of cold forging lubricants. *J. Mater. Process. Technol.*, 2007, **189**, 36–44.

3 **Nakamura, T., Bay, N.,** and **Zhang, Z. L.** FEM simulation of a friction testing based on combined forward conical can-backward straight can extrusion. *ASME, J. Tribol.*, 1998, **120**, 716–723.

4 **Ngaile, G., Jaeger, S.,** and **Altan, T.** Lubrication in tube hydroforming (THF). Part II. Performance evaluation of lubricants using LDH test and pear-shaped tube expansion test. *J. Mater. Process. Technol.*, 2004, **146**, 116–123.

5 **Ngaile, G., Jaeger, S.,** and **Altan, T.** Lubrication in tube hydroforming (THF). Part I: Lubrication mechanisms and development of model tests to evaluate lubricants and die coatings in the transition and expansion zones. *J. Mater. Process. Technol.*, 2004, **146**, 108–115.

6 **Ngaile, G.** and **Yang, C.** Analytical model for characterizing the pear-shaped tribotest for tube hydroforming. Part 1. *Proc. IMechE, Part B: J. Engineering Manufacture*, 2008, **222**(B7), 849–864.

7 **Ngaile, G., Cochran, J.,** and **Stark, D.** Formulation of polymer-based lubricant for metal forming. *Proc. IMechE, Part B: J. Engineering Manufacture*, 2007, **221**, 559–569.

APPENDIX

Notation

K	strength coefficient
L	linear section length
n	strain hardening exponent
PH	protrusion height of deformed tube
ΔPH	protrusion height change
Pi/p	internal pressure
r	outer radius of tube
rr	corner radius of tube
t	deformed tube thickness
t_0	initial tube thickness
α	centre angle of arc section
ε_N	hoop strain at the intersection between arc and linear sections
ε_Q	hoop strain at the free expansion zone
λ	ratio of outer radius to tube thickness
μ	friction coefficient
ϕ	outer diameter of tube
ψ	vertex pear-shaped die angle